The Contribution of Pre-impact Posture on Restrained Occupant Finite Element Model Response in Frontal Impact.

David Poulard, Damien Subit, Bingbing Nie, Jean-Paul Donlon, Richard.W Kent

The Contribution of Pre-impact Posture on Restrained Occupant Finite Element Model Response in Frontal Impact

DAVID POULARD[1], DAMIEN SUBIT[2], BINGBING NIE[1], JOHN-PAUL DONLON[1], and RICHARD W. KENT[1]

[1]*University of Virginia, Center for Applied Biomechanics, Charlottesville, Virginia*
[2]*Institut de Biomécanique Humaine Georges Charpak, Arts et Métiers ParisTech, Paris, France*

Objective: The objective of this study was to discuss the influence of the pre-impact posture to the response of a finite element human body model (HBM) in frontal impacts.

Methods: This study uses previously published cadaveric tests (PMHS), which measured six realistic pre-impact postures. Seven postured models were created from the THUMS occupant model (v4.0): one matching the standard UMTRI driving posture as it was the target posture in the experiments, and six matching the measured pre-impact postures. The same measurements as those obtained during the cadaveric tests were calculated from the simulations, and biofidelity metrics based on signals correlation (CORA) were established to compare the response of the seven models to the experiments.

Results: The HBM responses showed good agreement with the PMHS responses for the reaction forces (CORA $= 0.80 \pm 0.05$) and the kinematics of the lower part of the torso but only fair correlation was found with the head, the upper spine, rib strains (CORA$=$ 0.50 ± 0.05) and chest deflections (CORA $= 0.67 \pm 0.08$). All models sustained rib fractures, sternal fracture and clavicle fracture. The average number of rib fractures for all the models was 5.3 ± 1.0, lower than in the experiments (10.8 ± 9.0).

Variation in pre-impact posture greatly altered the time histories of the reaction forces, deflections and the rib strains, mainly in terms of time delay, but no definite improvement in HBM response or injury prediction was observed. By modifying only the posture of the HBM, the variability in the impact response was found to be equivalent to that observed in the experiments. The postured HBM sustained from 4 to 8 rib fractures, confirming that the pre-impact posture influenced the injury outcome predicted by the simulation.

Conclusions: This study tries to answer an important question: what is the effect of occupant posture on kinematics and kinetics. Significant differences in kinematics observed between HBM and PMHS suggesting more coupling between the pelvis and the spine for the models which makes the model response very sensitive to any variation in the spine posture. Consequently, the findings observed for the HBM cannot be extended to PMHS. Besides, pre-impact posture should be carefully quantified during experiments and the evaluation of HBM should take into account the variation in the predicted impact response due to the variation in the model posture.

Keywords: biomechanics, injury outcome, seat belt, modeling, impact responses, biofidelity

Introduction

Although significant improvements have been achieved in mitigating road traffic fatalities, frontal impacts play a predominant role in the frequency of road traffic fatalities (Nirula and Pintar 2008). Since the early 1960s, the goal of reducing chest injuries has motivated numerous studies of human thoracic response to frontal loadings (Backaitis 1994; Kroell et al. 1971).

Associate Editor Joel Stitzel oversaw the review of this article.
Address correspondence to David Poulard, University of Virginia, Center for Applied Biomechanics, 4040 Lewis & Clark Drive, Charlottesville, VA 22911. E-mail: dp5fv@virginia.edu
Color versions of one or more of the figures in the article can be found online at www.tandfonline.com/gcpi.

In frontal crashes, thoracic deformation due to anterior chest loading is generally accepted as the parameter that best correlates to the rib and sternal fractures, as well as the most frequently observed thoracic injury for occupants in vehicles equipped with contemporary restraint systems (Kent et al. 2003). Consequently, improved biofidelity of the torso-to-restraint loading remains a priority for advanced human body models. A simulated impact (sled test) provides the most realistic conditions for defining human response (as approximated by cadavers, the best available human surrogate for injurious impact tests; Crandall et al. 2011) and, therefore, for assessing chest biofidelity. Such tests are the primary source of data for the development of anthropometric test devices and for the validation and development of finite element (FE) models (HBMs; Poulard, Kent, et al. 2015).

In a recent series of sled tests, 8 restrained postmortem human subjects (PMHS) were subjected to 40 km/h frontal impacts (Shaw et al. 2009). Extensive measurements were taken during the impact, including measurements of the positions of several bones immediately prior to impact. In the current study, this set of measurements is referred to as the *pre-impact posture*. The number of rib fractures documented varied from 2 to 27, and no correlation could be found between the number of fractures and the bone mechanical strength. It was hypothesized that the pre-impact posture of the subjects could play an important role in the reported variability by modifying the load path to the ribcage. Because the test subjects in the study had different anthropometries and pre-impact posture, the contribution of the pre-impact posture to the mechanical response is unknown. Compared to experimental tests performed with PMHS, simulations with computational human models have the potential to evaluate the impact response of a single individual while introducing extrinsic variability (Poulard et al. 2014).

Therefore, the objective of the study was to analyze independently the contribution of pre-impact posture to impact response by subjecting a single FE HBMs with different pre-impact postures to identical frontal sled tests. This approach was used previously to study the influence of pre-impact postures in side impacts (Poulard et al. 2014). The model response was compared to the PMHS responses using an objective assessment tool to confirm that the trends observed were relevant.

Materials and Methods

Overview of the Experiments

Eight male PMHS with approximately 50th percentile stature and mass were tested in a 40 km/h frontal sled test that used a 14 *g* trapezoidal deceleration and 3-point restraint (Shaw et al. 2009). The condition was selected to represent a repeatable pure frontal collision in the severity range of regulatory frontal impact tests (e.g., FMVSS-208) (Hollowell et al. 1999) using a standard non-force-limiting 3-point belt. No retractor was used in the shoulder belt in order to maximize repeatability and minimize variation. Additional restraint for the pelvis and lower extremities was provided by a rigid knee bolster (adjusted to be in contact with the knees at the time of impact) and a footrest. Restraint and surface interactions were recorded using load cells.

Data collected at 1,000 fps from an optically based motion capture system during the tests were used to calculate the 6-degree-of-freedom motion of the head, first thoracic vertebra (T1), eighth thoracic vertebra (T8), second lumbar vertebra (L2), fourth lumbar vertebra (L4), and pelvis of each subject relative to the vehicle buck. The images from the pre-instrumentation computed tomography scans were then segmented to produce 3-dimensional reconstructions of the target bones (Figure D1, see online supplement). The motions of the bones were prescribed from the experimental data to create 3-dimensional kinematic animations (3DKA) of the tests using the method described in Donlon et al. (2015).

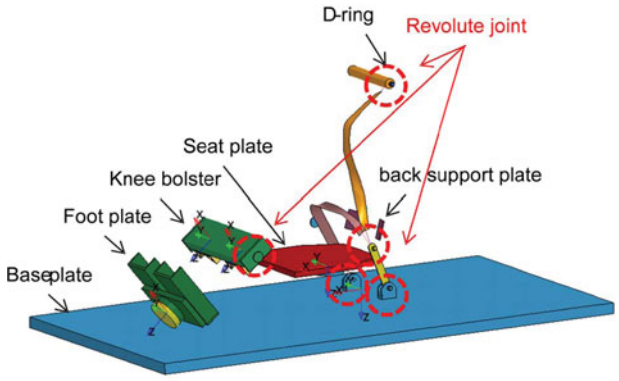

Fig. 1. Buck model.

Additional subject instrumentation included 6-axis accelerometers and angular rate sensors located in the head, T1, T8, L2, L4, and pelvis. Three subjects were also instrumented with strain gages glued to the sternum, right clavicle, and ribs 3, 5, and 7.

Results of these tests have been reported previously in the form of chest deformation (Shaw et al. 2009), spine kinematics (Crandall et al. 2014), and restraint/support forces (Ash et al. 2013).

Six tests, which are a subset of those presented by Shaw et al. (2009), were selected as examples of realistic pre-impact postures (Figure D1 and Table B1, see online supplement). For each subject, the pre-impact leaning of the spine was defined by the lateral leaning angle θ_L measured in the frontal plane and a sagittal leaning angle θ_F measured in the saggital plane. Both angles were defined from the local origin of the pelvis (the midpoint of the posterior superior iliac spines) and the local origin of the T1 vertebra (the midpoint of the centers of the superior and inferior endplates).

Environment Model

The computational model of the buck was developed based on 3D CAD drawings (Figure 1). A number of key components were modeled as rigid bodies (base plate, seat plate, back support plate, D-ring, outboard anchor, inboard anchor, rod, buckle, foot plate, and knee bolster). The load cells in the foot plate, knee bolster, and seat plate were replicated using beam elements that can measure the 6-degree-of-freedom reaction force (*Fx*, *Fy*, *Fz*, *Mx*, *My*, and *Mz*). In addition, rotational joints were used to connect the D-ring, knee bolster, inboard anchor, outboard anchor, and buckle to the frame to allow their rotation relative to the frame (Figure 1).

The webbing characteristics published in Shaw et al. (2009) were discretized and used in the seat belt material definition (6–8% elongation, 10.7 kN tensile strength). The belt load path was defined using the LS-Prepost Seatbelt Fitting tool (Livermore, CA). The waypoints used to define the belt path were the same among the postured models. The position of the D-ring was adjusted to ensure that the angle of the shoulder belt in the sagittal plane between the vertical direction and the shoulder was 27° (average value in the experiments). The

postured models were positioned with respect to the seat so that the H-point position relative to the seat was constant across models.

The models were subjected to a prescribed deceleration defined as the average trapezoidal pulse obtained in the experiments (Ash et al. 2013).

Human Body Model Instrumentation

The HBM used in the present study was THUMS version 4.0, 50th percentile male, 175 cm and 76 kg (Shigeta et al. 2009). The model was instrumented for comparison with experiments.

Three-dimensional displacement of the head, spine (T1, T8, L2, and L4), and pelvis relative to the vehicle coordinate system were measured from the model. The anatomical centers were defined according to Wu et al. (2005) following the method described in a previous study (Poulard et al. 2014).

Triaxial accelerations were measured using a $2 \times 2 \times 2$ mm aluminum cube rigidly attached to the center of the bony location (head, T1, T8, L2, L4, and pelvis).

Rib strains were measured on the model by outputting strains in the corresponding element on the cortical part of the bone (layered with shells). The corresponding element was identified to correspond to the average position in the experiments (taking into account the difference in anthropometries across PMHS).

The main injuries to be predicted in simulation were bone fractures of the ribs, sternum, scapula, and clavicles, which were predicted in postprocessing from ultimate plastic strain values in the bone structures. The threshold of the ultimate plastic strain values for bone fractures was varied from 3% (representing 20 years old) to 0.8% (representing 75 years old) to study the effect of age by using the equation developed by Golman et al. (2014).

Applying Pre-impact Posture

The method used to adapt the pre-impact posture was described in a previous study (Poulard, Subit, et al. 2015). It involved pulling cables to prescribe the position and orientation of T1 and pelvis during a simulation (Figure D2, see online supplement). Each pulling system consisted of a cable, 2 rigid plates in aluminum, a spring, and a slipring. One plate was linked by the spring to the part to be moved (plate 1) and the other plate was fixed to the target location (plate 2). The 2 plates had the same orientation. One end of the cable was fixed to plate 1, and the other end was driven by a prescribed acceleration. A slip ring anchored to plate 1 and a contact between the 2 plates prevented plate 2 from moving past plate 1. By combining 3 pulling systems, both the final position and the final orientation of a body segment could be controlled.

For each bony segment, the 3 targets used to determine its position and orientation were the extremities of the vectors that define the local coordinate system (Figure D2). The positions of these landmarks were the targets used to position THUMS and were normalized in order to account for the difference in spine length and anatomy between THUMS and the PMHS (Poulard, Subit, et al. 2015).

Table 1. Postured model IDs and associated leaning angles (sagit-tal: θ_F, l a t e r a l : θ_L) after the postural change

Models	Associated test IDs	θ_F Target	θ_F Obtained	θ_L Target	θ_L Obtained	Reference
HBM_F0	None	None	76.0	None	0.0	Reference posture
HBM_F1	1294	78.0	78.3	1.7	1.7	Shaw et al. (2009)
HBM_F2	1295	82.1	82.5	−1.6	−1.6	Shaw et al. (2009)
HBM_F3	1358	74.8	74.5	1.2	1.1	Shaw et al. (2009)
HBM_F5	1360	75.0	74.8	−2.3	−2.2	Shaw et al. (2009)
HBM_F6	1378	70.5	70.6	−2.2	−2.2	Shaw et al. (2009)
HBM_F8	1380	70.4	70.4	−1.2	−1.1	Shaw et al. (2009)

The simulation was stopped when the spine posture was acceptably close to the desired curvature and the soft tissues were stabilized (no observable deformations). The desired curvature was reached quickly (at 150 ms), whereas it took longer for the soft tissues to stabilize (about 300 ms). At the end of the simulation, the nodal coordinates of the model (excluding the posture apparatus) were exported.

Additional presimulations were performed to adjust the lower extremities toward the average angle obtained in experiments and to put the arms in contact with the thighs. Before the impact simulation was run, the HBM was allowed to settle on the buck using gravity, and strains and stresses due to gravity were accounted for at this time. Simulation was stopped when the oscillations in the contact force amplitude between the HBM and the seat decreased below 2%. The nodes of the HBM and the strains and stresses were exported from the final state and were included in the impact simulations. At the beginning of the impact, the resultant contact force between the seat and the HBM was 751 ± 11 N ($n = 7$).

Seven postured models were created from the original THUMS (Figure 2): one matching the standard University of Michigan Transportation Research Institute driving posture (posture F0) because it was the target in the experiments and 6 matching the pre-impact posture measured for each of the 6 selected subjects, called postures F1–F8 (Table 1). The average error between the target angle and the obtained angle after application of the method were satisfactory (θ_F: $0.2 \pm 0.1^\circ$; θ_L: $0.1 \pm 0.1^\circ$). All postured models (F1–F8) met mesh quality guidelines described in the THUMS manual and were comparable to the baseline THUMS baseline model (F0).

Each of these models and the baseline model were subjected to sled tests.

Quantitative Assessment of the Response of the Model

A quantitative assessment of the response of the models compared to the experiments was performed through metrics obtained with the CORA software (CORelation and Analysis, Parternship for Dummy Technology and Biomechanics; Gehre et al. 2009). Each of these metrics, including the corridor, phase, magnitude, and slope, is given a subscore and the weighted sum of these subscores is the CORA score ranging between 0 and 1. The weighting factors of the subscores are 0.4 for the corridor, 0.2 for the phase, 0.2 for the magnitude, and 0.2 for the slope (ISO/TS 18571 in Barbat et al. 2013). A CORA score above 0.8 is considered to be a good fit between

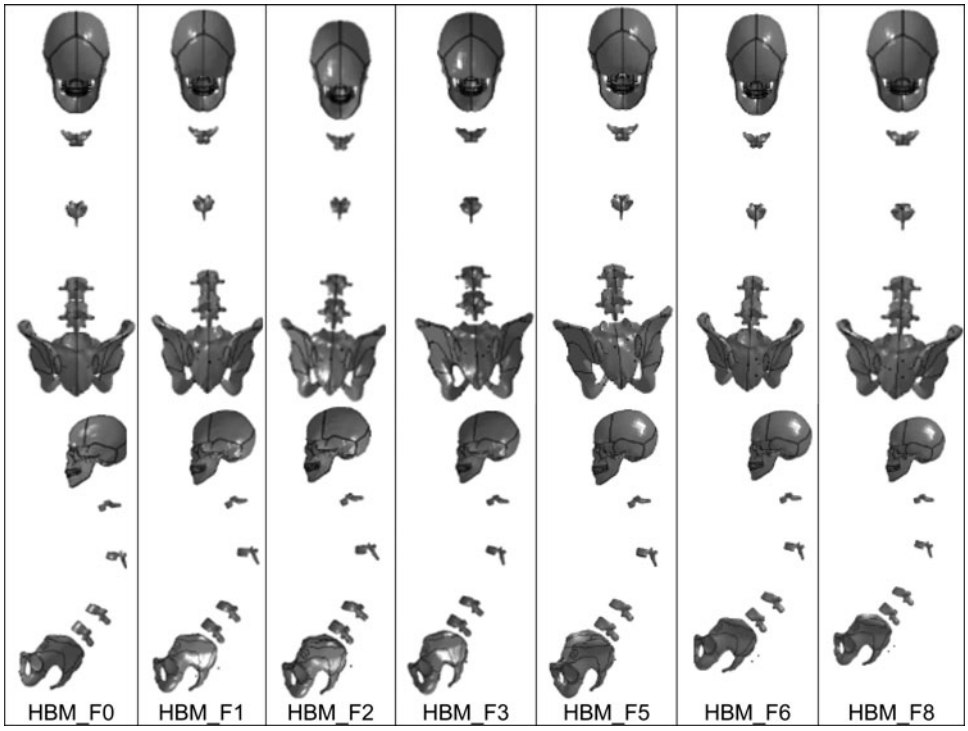

Fig. 2. Postured models.

the model and the experiments (Barbat et al. 2013). Because CORA calculates the correlation of each signal separately, those single ratings were combined into a global model rating by calculating the mean value of all the ratings. Table B2 (see online supplement) shows which data (i.e., signal) were used to establish the rating. The full set of parameters used in CORA is provided in Appendix C (see online supplement).

All experimental corridors have been previously reported in the form of chest deformation (Shaw et al. 2009), kinematics (Crandall et al. 2014; Lessley et al. 2014), and restraint/support forces (Ash et al. 2013). For a given parameter the response data were averaged for each point in time and then a ± 1 standard deviation corridor was generated around the average response curve. Kinematics corridors were developed according to the method described in Lessley et al. (2014), which also included the differences in time considering the standard deviation of the responses in both axes. The corridor score was calculated using the actual experimental standard deviation.

Descriptive Analyses

The parameters in this study were the CORA scores obtained for the models and the time and amplitude of peak outputs: force, acceleration, rib strains, and deflections. Descriptive statistics were given for all parameters as mean $\pm$ one standard deviation (S.D.).

Results

Kinematics

Displacement time history plots for all models are provided in Figure A7 (see online supplement) and compared to their respective corridors for the selected measurement locations. For each measurement location plots are provided for the X-axis, Y-axis, and Z-axis skeletal displacement relative to the vehicle buck. The displacement magnitude was greatest in the positive X-axis direction and was observed to be the highest at the head, with progressively decreasing magnitudes occurring at inferior locations along the spine from T1 to the pelvis. All locations along the spine moved upward (negative Z-axis direction) during the simulation with the exception of the head, which moved downward (positive Z-axis direction). Similar patterns were observed between experiments and the models for the pelvis, L4, and L2. Significant differences were observed for T8, T1, and the head. The predominate displacements were observed to occur within the saggital (X–Z) plane as in the experiments; however, less displacement was observed in the X-axis for the head (HBM: 272 $\pm$ 19 mm, PMHS: 383 $\pm$ 63 mm). The mean peak displacement in the X-axis, Y-axis, and Z-axis directions for each measurement location are provided as a bar chart in Figure D3 (see online supplement), and Figure 3 illustrates the difference in head rotation between the model and experiment.

Forces

Force–time history plots for all models are provided in Figure A1 (see online supplement) and compared to their respective corridors. The force–time histories predicted in the simulations were similar to those observed in the experiments. Quantitatively, no significant difference was observed between the models ($n = 7$) and experiments ($n = 6$) in terms of phase and amplitude (Table 2; Figure D4, see online supplement).

The average CORA model score for forces was 0.80 ± 0.05 ($n = 7$), showing good overall correlation (Table B3, see online

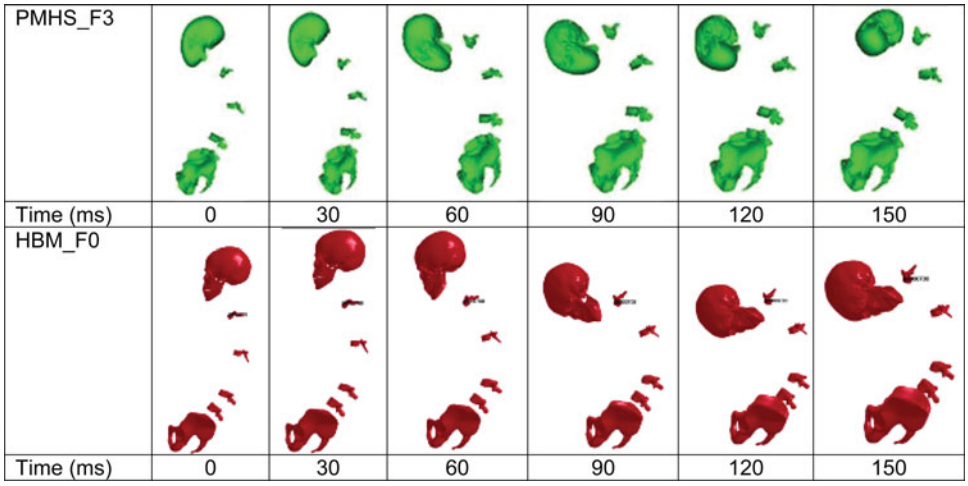

Fig. 3. Comparison of kinematics between the baseline model (bottom) and PMHS (top).

supplement). Variability was observed between the average CORA score obtained for the upper should belt load (0.95 ± 0.03) and the average CORA score obtained for the footrest (0.53 ± 0.15).

The initial posture was found to affect both phase and amplitude of forces (Table 2). Though CORA scores were able to reflect the variability induced by the alteration of posture (CORA scores ranges from 0.70 to 0.85), the model scores were not improved after the alteration of posture.

Accelerations

Acceleration time history plots for the head, T1, T8, L2, L4, and the pelvis are provided in Figure A2 (see online supplement). The acceleration time histories predicted in the simulations were similar to those observed in the experiments. Quantitatively, no significant difference was observed between the models ($n = 7$) and experiments ($n = 6$) in terms of phase and amplitude (Table 2; Figure D4). As a general trend, peak accelerations were reached earlier in the models than in the experiments (especially T8 and T12) and the average peak resultant for the head was lower (HBM: 40.2 ± 15.5 *g*, PMHS: 67.8 ± 16.0 *g*).

The average CORA model score for resultant acceleration, all body segments combined, was 0.67 ± 0.05 ($n = 7$), indicating a fair overall correlation (Table B3). Low variability was observed among body segments; the lower average score was 0.64 ± 0.03 for T8 and the highest was 0.71 ± 0.03 for the pelvis.

The initial posture was found to affect both phase and amplitude of the acceleration (Table 2). Though CORA scores were able to reflect the variability induced by the alteration of posture (CORA scores ranges from 0.61 to 0.77), the model scores were not improved after the alteration of posture.

Rib Strains

Time histories for each gauge over the time interval from 0 to 150 ms are shown in Figure A3 (see online supplement). Tension is indicated by a positive value. The models predicted strain patterns that differed from those observed in the corridors defined from three subjects. The model was not able to capture the abrupt variations observed in the rib corridors at 60 ms for rib 5R lateral and rib 7R medial, which was due to rib fracture happening for 2 of the tests (Shaw et al. 2009). As a general trend, the amplitude of strain was underestimated by the model compared to the experiments especially for rib 3R (HBM: 0.21 ± 0.08%, PMHS: 1.01 ± 0.64%), rib 5R lateral (HBM: 0.13 ± 0.06%, PMHS: 0.49 ± 0.08%), and rib 7L lateral (HBM: 0.14 ± 0.06%, PMHS: 0.87 ± 0.20%).

The average CORA model score for strains, all gages combined, was 0.50 ± 0.05 ($n = 7$), indicating a fair overall correlation (Table B3). High variability was observed between rib segments; the lower average score was 0.43 ± 0.05 for rib 5L–lateral and the highest was 0.67 ± 0.01 for rib 7R–lateral.

The initial posture was found to affect both the phase and amplitude of rib strains (Table 2). Though CORA scores were able to reflect the variability induced by the alteration of posture (CORA scores ranges from 0.43 to 0.59), the model scores were not improved after the alteration of posture.

Torso Deformation

Figure A4 (see online supplement) presents the time–histories of the 3D anterior ribcage displacements relative to the T8 coordinate system X, Y, and Z axes. Though the models predicted torso deformation that were similar to those observed in the experiments in term of shape, the amplitudes of deflections were underevaluated by the model. Quantitatively, a difference was observed between the models ($n = 7$) and experiments ($n = 6$) in terms of amplitude and phase for the peak deflections for the upper left (HBM: 20.6 ± 8.8 mm, PMHS: 50.3 ± 24.6 mm).

The average CORA model score for deflections is 0.67 ± 0.08, showing overall fair correlation (Table B3). Variability was observed along the ribcage; the lower average score was 0.63 ± 0.13 for the upper right of the ribcage and the highest was 0.72 ± 0.04 for the lower right.

Table 2. Timing and amplitude of peak signals obtained by models (HBM) and PMHS

		Models								Experiments		
		HBM_F0	HBM_F1	HBM_F2	HBM_F3	HBM_F5	HBM_F6	HBM_F8	Average ($n = 7$)	SD	Average ($n = 6$)	SD
						Forces						
Seat	Peak (N)	4,680	5,104	,5429	4,837	5,459	5,324	5,920	*5,250*	*417.7*	4,292	753.8
	Time of peak (ms)	42.5	49.8	51.0	46.8	50.4	57.1	51.6	*49.9*	*4.5*	43.7	9.7
Footrest	Peak (N)	5,181	5,260	4,948	5,155	5,213	6,119	5,548	*5,346*	*384*	4,735	938.2
	Time of peak (ms)	51.1	54.0	54.6	45.6	55.0	68.9	59.4	*55.5*	*7.3*	46.77	0.804
Knee bolster	Peak (N)	3,659	4,472	5,873	2,929	2,935	3,542	3,133	*3,792*	*1,064*	5,047	983.1
	Time of peak (ms)	30.7	48.9	41.5	50.0	52.6	51.7	48.1	*46.2*	*7.7*	41.4	2.5
Upper shoulder belt	Peak (N)	6,902	6,832	7,322	6,554	6,531	6,399	6,552	*6,727*	*316.9*	6,377	679.4
	Time of peak (ms)	99.3	95.8	88.9	85.7	85.7	108.2	103.5	*95.3*	*8.9*	93.9	11.0
Lower shoulder belt	Peak (N)	5,390	5,250	5,474	5,495	5,922	4,578	4,522	*5233*	*510.0*	5,346	329.4
	Time of peak (ms)	104.7	96.3	88.4	85.8	84.4	88.5	87.9	*90.9*	*7.2*	90.0	6.2
Lap belt	Peak (N)	671	1,070	1,030	940	996	1,100	1,010	*974*	*143.2*	809.5	207.8
	Time of peak (ms)	42.9	53.4	55.5	52.4	53.2	56.9	54.6	*52.7*	*4.6*	57.3	13.54
						Accelerations						
Head	Peak resultant (*g*)	28.0	27.6	63.1	52.2	53.5	26.1	30.6	*40.2*	*15.5*	67.8	16.0
	Time of peak (ms)	81.3	126.5	127.1	88.1	88.3	126.4	86.3	*103.4*	*21.9*	103.6	21.8
T1	Peak resultant (*g*)	18.3	18.7	17.5	27.8	40.1	23.7	21.5	*23.9*	*8.0*	39.8	11.3
	Time of peak (ms)	59.6	70.5	53.8	73.4	141.1	54.1	68.0	*74.4*	*30.4*	78.7	7.7
T8	Peak resultant (*g*)	24.1	23.0	22.0	29.3	33.1	36.4	37.0	*29.3*	*6.4*	29.2	2.7
	Time of peak (ms)	41.4	62.2	82.5	72.2	46.1	48.6	70.1	*60.4*	*15.4*	78.9	17.1
L2	Peak resultant (*g*)	29.0	28.2	31.5	32.2	28.8	48.3	30.9	*32.7*	*7.0*	27.2	2.9
	Time of peak (ms)	43.0	44.9	65.8	56.5	73.0	53.9	67.2	*57.8*	*11.4*	73.4	24.8
L4	Peak resultant (*g*)	19.8	22.6	28.1	24.2	36.8	24.6	26.9	*26.1*	*5.4*	26.0	6.2
	Time of peak (ms)	40.7	35.0	64.0	56.5	124.2	40.5	67.3	*61.2*	*30.5*	65.1	32.5
Pelvis	Peak resultant (*g*)	13.0	19.6	23.8	21.1	21.3	21.3	26.6	*21.0*	*4.2*	20.7	2.6
	Time of peak (ms)	34.5	35.4	37.6	56.5	57.9	67.4	32.1	*45.9*	*14.2*	59.4	27.4
						Deflections						
Sternum	Peak (mm)	45.4	37.4	77.1	27.9	14.6	24.6	28.5	*36.5*	*20.4*	*66.6*	*21.1*
	Time of peak (ms)	93.0	76.0	91.0	49.0	59.0	79.0	79.0	*75.1*	*16.0*	*102.0*	*12.0*
Upper left	Peak (mm)	29.3	26.8	32.8	13.4	12.9	11.5	17.7	*20.6*	*8.8*	*50.3*	*24.6*
	Time of peak (ms)	92.0	85.0	86.0	49.0	59.0	62.0	132.0	*80.7*	*27.8*	*103.0*	*15.3*
Upper right	Peak (mm)	20.3	6.8	30.2	6.4	9.3	38.4	38.1	*21.3*	*14.3*	*35.1*	*11.1*
	Time of peak (ms)	119.0	89.0	99.0	49.0	59.0	79.0	82.0	*82.3*	*23.6*	*107.0*	*19.5*
Lower left	Peak (mm)	22.1	20.0	20.1	15.0	7.7	55.6	71.9	*30.4*	*23.8*	*48.9*	*17.0*
	Time of peak (ms)	68.0	76.0	99.0	49.0	43.0	79.0	75.0	*69.9*	*19.0*	*104.0*	*16.1*
Lower left	Peak (mm)	54.0	50.7	35.2	16.6	46.2	71.7	72.3	*49.5*	*19.7*	*56.6*	*21.4*
	Time of peak (ms)	72.0	80.0	73.0	49.0	59.0	79.0	79.0	*70.1*	*11.8*	*114.0*	*12.4*
						Strain						
Rib 3R–medial	Peak (SI)	0.31%	0.30%	0.23%	0.19%	0.21%	0.09%	0.15%	0.21%	0.08%	1.01%	0.64%
	Time of peak (ms)	73.6	78.8	72.3	56.6	62.3	62.8	105.4	73.1	16.2	106.9	66.8
Rib 5R–medial	Peak (SI)	0.37%	0.35%	0.15%	0.22%	0.26%	0.43%	0.46%	0.32%	0.12%	0.58%	0.30%
	Time of peak (ms)	121.3	93.7	82.3	50.2	62.3	85.7	81.1	82.4	22.7	146.6	86.3
Rib 5R–lateral	Peak (SI)	0.15%	0.13%	0.13%	0.04%	0.06%	0.18%	0.20%	0.13%	0.06%	0.49%	0.08%
	Time of peak (ms)	121.4	92.7	102.6	57.7	62.3	85.9	90.1	87.5	22.1	83.0	20.1
Rib 7R–medial	Peak (SI)	0.34%	0.35%	0.27%	0.27%	0.39%	0.42%	0.44%	0.36%	0.07%	0.43%	0.12%
	Time of peak (ms)	82.1	76.5	76.2	56.2	62.3	78.3	69.5	71.6	9.4	75.4	18.2
Rib 7R–lateral	Peak (SI)	0.23%	0.20%	0.18%	0.24%	0.29%	0.28%	0.30%	0.25%	0.05%	0.41%	0.32%
	Time of peak (ms)	64.6	66.4	61.2	56.7	62.3	68.8	63.5	63.4	3.9	102.0	49.3
Rib 5L–medial	Peak (SI)	0.38%	0.39%	0.41%	0.28%	0.20%	0.29%	0.19%	0.30%	0.09%	1.20%	0.62%
	Time of peak (ms)	84.6	87.0	82.8	57.7	59.8	56.6	132.0	80.1	26.6	138.1	71.7
Rib 5L–lateral	Peak (SI)	0.20%	0.20%	0.26%	0.20%	0.17%	0.18%	0.20%	0.20%	0.03%	0.82%	0.30%
	Time of peak (ms)	91.4	61.9	87.6	56.5	57.0	85.0	79.3	74.1	15.2	97.8	15.1
Rib 7L–medial	Peak (SI)	0.28%	0.30%	0.33%	0.15%	0.09%	0.14%	0.20%	0.21%	0.09%	0.83%	0.36%
	Time of peak (ms)	99.4	96.6	83.6	57.7	62.3	59.8	132.3	84.5	27.3	108.6	21.3
Rib 7L–lateral	Peak (SI)	0.17%	0.16%	0.18%	0.07%	0.06%	0.12%	0.23%	0.14%	0.06%	0.87%	0.20%
	Time of peak (ms)	95.2	97.4	83.9	57.7	61.6	87.2	78.8	80.3	15.5	98.1	9.2
Clavicle	Peak (SI)	0.29%	0.23%	0.08%	0.04%	0.03%	0.50%	0.40%	0.22%	0.18%	0.57%	0.08%
	Time of peak (ms)	129.8	79.4	98.2	57.7	40.3	88.5	98.6	84.6	29.3	85.8	4.5
Sternum	Peak (SI)	0.32%	0.31%	0.58%	0.24%	0.24%	0.17%	0.21%	0.30%	0.14%	0.60%	0.23%
	Time of peak (ms)	72.7	74.9	98.7	57.7	62.3	60.3	57.8	69.2	14.7	74.2	11.1

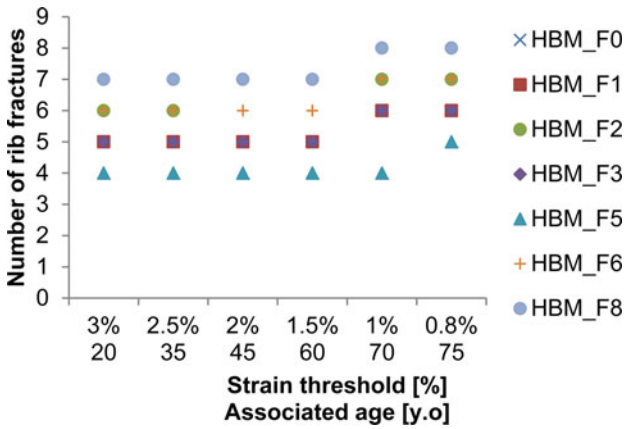

Fig. 4. Number of rib fractures obtained for the differently postured models according to various ultimate strain thresholds and associated ages.

The initial posture was found to have a significant effect on deflections, which affected both phase and amplitude (Table 2). Though CORA scores were able to reflect the variability induced by the alteration of posture (CORA scores ranges from 0.52 to 0.74), the model scores were not improved after the alteration of posture.

Injury Outcome

Table B4 (see online supplement) provides a summary for the injury outcome for both postured models with 3% threshold and experiments. All models sustained rib fractures, sternal fracture, and clavicle fracture. The average number of rib fractures for all models was 5.3 ± 1.0, lower than in the experiments (10.8 ± 9.0). The initial posture was found to have a significant effect on deflections because the number of rib fractures ranged from 4 (HBM_F5) to 7 (HBM_F8). The injury outcome was not improved after the alteration of the posture; the lowest rib fracture observed in experiments (PMHS_F8) is associated with the highest value of number of rib fractures in simulations (HBM_F8).

In Table B5 (see online supplement), the ultimate plastic strain range was adjusted from 3.00% (representing 20 years old) to 0.8% (representing 75 years old) according to the equation developed by Golman et al. (2014). An average increase of one additional rib fracture was observed between 3% (5.4 ± 1.0) and 0.8% (6.4 ± 1.0; Figure 4).

Discussion

Evaluation of Model Biofidelity for Frontal Impact

The goal of this study was to analyze the influence of pre-impact posture on the impact response of PMHS. This study can be only performed using HBM under injurious test conditions because PMHS differed in anthropometries and age. Nevertheless, by using HBM, the evaluation of the influence of pre-impact posture focused on HBM and not PMHS. Consequently, the evaluation of the model biofidelity for frontal impact was included in the present study to ensure that the trends observed for the HBM are relevant.

The HBM responses showed good agreement with the PMHS responses for the reaction forces and the kinematics of the lower part of the torso but only fair correlation was found with the head, upper spine, and ribcage deformation.

The head model did not exhibit rotation around the vertical axis contrary to the experiments, which affected the kinematics and may have affected the load path and the injury outcome. Different parameters, such as neck muscle modeling in THUMS and neck and head anatomical differences between THUMS and the PMHS (as the head weight, not reported in the experiments) may have played a role in this behavior discrepancy.

The model was found to underpredict the peak strain for all areas compared to the average experimental response. Different hypotheses can explain this behavior. The number of samples ($n = 3$) for the rib strains defining the average experimental response was found to limit the comparison because great variability was observed in the experiments corridors. In addition, the belt path used in the current study is the average belt path reported in Shaw et al. (2009). Though it was necessary to limit the number of parameters evaluated in the study (posture, age), an average belt path may not encompass the variability observed in experiments because different belt path can generate different patterns of response. Finally, the ribcage of the model may be too stiff compared to the average experimental response, which prevented significant local deformation from happening and tended to distribute the energy all along the ribcage. It will be interesting to conduct local tests (rib 3-point bending tests, ribcage point loading, etc.) on the HBM to evaluate local compliance.

The CORA evaluation was used to combine a large set of results and ensure that the response of the model after alteration of the posture was valid. CORA scores above 0.8 were associated with a good fit between the model and the results. This choice of threshold, though mostly arbitrary, is supported by previous studies (Poulard, Kent, et al. 2015; Poulard et al. 2014; Vavalle et al. 2013). A lack of interpretation for the ratings between 0.5 and 0.8 was also previously noted (Poulard et al. 2014), which limited the use of CORA of any absolute classification of an HBM. A relative assessment of different versions of the same model using CORA seems more pertinent that an absolute evaluation of a specific version. In the current study, corridor score, which is the most contributing score in CORA, was calculated using the actual experimental standard deviation instead of as a percentage of trace as stipulated in ISO/TS 18571. In the first phase of the analysis, the 2 methods were investigated and the corridors generated using ISO/TS 18571 were found to be wide enough to enclose all responses (corridors scores that were above 0.8 with ISO) even for specific outputs that were significantly different were from the experiments (deflections and rib strains). Using the standard deviation, the corridors scores were lower and judged more exploitable.

In the current study, we decided to evaluate the injury prediction using postprocessing (no element elimination) to ensure numerical stability of the model. The main reason was that explicitly simulating the injuries using failure, damage

functions, and element elimination was found to overestimate the number of rib fracture (Poulard et al. 2014). Hence, the mechanical response of an undamaged model might be different from an actual damaged model, which could explain why the model was not able to capture the abrupt variation in rib strains due to fracture in the experiments.

Influence of Pre-impact Posture

In the simulations, the pre-impact posture was found to alter the reaction forces, kinematics, and strains in the ribcage of the models. By only modifying the posture of the HBM, the variability (defined as the standard deviation) in the time of peak was found to be similar to that observed in the experiments performed with different PMHS. However, the alteration of the posture was found to have a limited effect on the amplitude of the outputs, which suggested that the alteration of anthropometries could play a greater role in this response. In this study, the CORA scores captured the variability induced by the alteration of posture but were not improved after the alteration of the posture. This may be due to the choice of parameters used in CORA (i.e., the weighting factors of the subscores) based on ISO/TS 18571, which give equal weights for time parameters (for which delays due to posture could be expected) and amplitude (for which mass differences that were not accounted for could affect the results). Because the PMHS were of different sizes than the HBM, it will be interesting to include geometrical personalization (morphing) in the next studies. An extension of this study—for example, where morphing is added to the differently postured HBM—is needed to evaluate how the anthropometries affect the prediction ability of the model. A parametric analysis to evaluate the effect of the posture in a systematic way would help to confirm the results presented in this article and allow the performance of statistical tests between postured models.

Though initial posture was found to play a role in the level of chest deflection and the number of rib fractures predicted by the model, it was reported that the same posture accounts for the lowest number of rib fractures observed experimentally (PMHS_F8, 2 rib fractures) and the highest number in the model (HBM_F8, 7 rib fractures). Because the subject and the HBM shared similar stature, which was close to the 50th percentile (PMHS: 180 cm, 78 kg; HBM: 177 cm, 77 kg) it was unlikely that the difference was due to anthropometry, assuming no local body differences. The belt path was also similar (belt crossing the mid-sternum and going mid-clavicle for both PMHS and model), so it was unlikely that the belt path would have played a role. The authors assumed that because the PMHS was young at his time of death (37 years old), his bone mineral density and consequently his toughness would be higher than the average value used in the model. Though the effect of age was included by adjusting the strain threshold in postprocessing, bone mineral density was not adjusted, which could explain the higher number of rib fractures predicted.

Furthermore, it does not necessarily mean that the findings observed for the HBM can be extended to PMHS. As stated above, significant differences in kinematics were observed between HBM and PMHS for different body regions, suggesting more coupling between the pelvis and the vertebrae for the models, which makes the impact response of the model very sensitive to any variation in the spine posture. The high coupling between the different body parts of the model was previously highlighted in whole-body side impact (Poulard et al. 2014). Consequently, though pre-impact posture influenced significantly the response of HBM, the contribution of pre-impact posture on PMHS could be lower. Nevertheless, the findings of this study highlight that the posture should be carefully quantified during experiments to allow a proper evaluation of models.

Finally, though the simulated environment used in this study provided realistic conditions for defining human response, it will be interesting to conduct a similar study with a frontal-impact airbag. It is expected that less variability in the model response would be observed because a fully deployed airbag will distribute the impact load over the whole body simultaneously.

Acknowledgments

The authors acknowledge Masao Muraji and Corinne Uskali (Toyota Motor Engineering & Manufacturing, North America) for their contribution to the design of the study.

Funding

This work was supported by funds from Toyota Collaborative Safety Research Center (Toyota CSRC). The experiments were funded by the NHTSA and the Japan Automobile Research Institute (JARI). The views expressed in this article are those of the authors and do not necessarily represent or reflect the views of the sponsors.

References

Ash J, Shaw G, Lessley D, Crandall J. PMHS restraint and support surface forces in simulated frontal crashes. *Int J Automot Eng.* 2013;4(2):41–46.

Backaitis SH. *Biomechanics of Impact Injury and Injury Tolerances of the Thorax–Shoulder Complex*. Warrendale, PA: Society of Automotive Engineers; 1994.

Barbat S, Fu Y, Zhan Z, Yang RJ, Gehre C. Objective rating metric for dynamic systems. Paper presented at: 21st International Technical Conference on the Enhanced Safety of Vehicles; May 27–30, 2013; Seoul, Republic of Korea.

Crandall JR, Bose D, Forman J, et al. Human surrogates for injury biomechanics research. *Clin Anat.* 2011;24:362–371.

Crandall J, Lessley D, Shaw G, Ash J. Displacement response of the spine in restrained PMHS during frontal impacts. *Int J Automot Eng.* 2014;5(2):59–64.

Donlon JP, Poulard D, Lessley D, Riley P, Subit D. Understanding how pre-impact posture can affect injury outcome in side impact sled tests using a new tool for visualization of cadaver kinematics. *J Biomech.* 2015;48:529–533.

Gehre C, Gades H, Wernicke P. Objective rating of signals using test and simulation responses. Paper presented at: 21st International Technical Conference on the Enhanced Safety of Vehicles; June 15–18, 2009; Stuttgart, Germany.

Golman AJ, Danelson KA, Miller LE, Stitzel JD. Injury prediction in a side impact crash using human body model simulation. *Accid Anal Prev.* 2014;64:1–8.

Hollowell WT, Gabler HC, Stucki SL, Summers S, Hackney JR. Updated Review of Potential Test Procedures for FMVSS no. 208. Washington, DC: Office of Vehicle Safety Research. National Highway Traffic Safety Administration (NHTSA); 1999.

International Organization for Standardization (ISO). Road vehicles – Objective rating metric for non-ambiguous signals. ISO/TS 18571; 2014.

Kent RW, Sherwood C, Lessley D, Overby B, Matsouka F. Age-related changes in the effective stiffness of the human thorax using four loading conditions. Paper presented at: International Research Council on the Biomechanics of Injury Conference; September 25–26, 2003.

Kroell C, Schneider D, Nahum A. Impact tolerance and response of the human thorax. In: *Biomechanics of Impact Injury and Injury Tolerances of the Thorax–Shoulder Complex*. Warrendale, PA: Society of Automotive Engineers. 1971:84–134.

Lessley D, Shaw G, Ash J, Crandall J. A methodology for assessing intrasegmental kinematics of the whole human spine during impacts. *Int J Automot Eng*. 2014;5(1):20144184.

Nirula R, Pintar FA. Identification of vehicle components associated with severe thoracic injury in motor vehicle crashes: a CIREN and NASS analysis. *Accid Anal Prev.* 2008;40:137–141.

Poulard D, Kent RW, Kindig M, Li Z, Subit D. Thoracic response targets for a computational model: a hierarchical approach to assess the biofidelity of a 50th-percentile occupant male finite element model. *J Mech Behav Biomed Mater.* 2015;45: 45–64.

Poulard D, Subit D, Donlon JP, Kent RW. Development of a computational framework to adjust the pre-impact spine posture of a whole-body model based on cadaver tests data. *J Biomech.* 2015;48: 636–643.

Poulard D, Subit D, Donlon JP, et al. The contribution of pre-impact spine posture on human body model response in whole-body side impact. *Stapp Car Crash J.* 2014;58:385–422.

Shaw G, Parent D, Purtsezov S, et al. Impact response of restrained pmhs in frontal sled tests: skeletal deformation patterns under seat belt loading. *Stapp Car Crash J.* 2009;53:1–48.

Shigeta K, Kitagawa Y, Yasuki T. Development of next generation human FE model capable of organ injury prediction. Paper presented at: 21st International Technical Conference on the Enhanced Safety of Vehicles Conference (ESV) - International Congress Center Stuttgart, Germany, June 15–18, 2009.

Vavalle NA, Jelen BC, Moreno DP, Stitzel JD, Gayzik FS. An evaluation of objective rating methods for full-body finite element model comparison to PMHS tests. *Traffic Inj Prev.* 2013;14(Suppl 1): S87–S94.

Wu G, Van Der Helm FC, Veeger HE, et al. ISB recommendation on definitions of joint coordinate systems of various joints for the reporting of human joint motion—Part II: shoulder, elbow, wrist and hand. *J Biomech.* 2005;38:981–992.